Effects of Boundary Conditions on Magnetic Friction

Kentaro Sugimoto

Department of Physics, The University of Tokyo

December 28, 2017

I would like to express my deepest gratitude to Prof. Naomichi Hatano whose enormous support and insightful comments were invaluable during the course of my study. I am also indebt to Ryo Tamura who provided technical help and sincere encouragement. I would also like to express my gratitude to my family for their moral support and warm encouragements.

Abstract

In the present thesis, hogehoge. Moreover, fugafuga.

Contents

Chapter 1

Introduction

In this chapter we introduce two of the most famous problems in analyzing the frictional force as the problem of statistical mechanics. We give recent developments for solving these problems. We then pose another problem regarding *manipulation* of the sliding friction which occurs in highly lubricated solids. To this end we simplify our problem into a dimensional crossover in lattice systems.

The sliding friction in solids is a very complicated problem to analyze, despite the fact that our daily lives are linked with it in various forms. One reason of the difficulty is that there is no general theory which determines the most important microscopic degree of freedom for the sliding friction as a macroscopic phenomenon.

One may think that with the skill of statistical mechanics we can deal with the problem in a systematic manner. However, there are several essential problems including the following: (1). The sliding friction is essentially non-equilibrium phenomenon (see Section1.1). (2). We cannot directly observe the sliding surface (see Section1.2).

1.1 Sliding Frictions as Non-Equilibrium Problems

We can regard the sliding friction the following elementary problem. We consider an object O and a substrate S, and let S slide against O by adding an external force. When O and S interact with each other, the kinetic energy of O given by the external force is expected to be lost through the interaction, and then the entire system $O + S$ heats up (if the system is closed) or the energy dissipates from the system to an external environment (if the system is open). In the latter case, under the assumption that the dissipation process is stationary, the frictional force takes a constant value balancing with the external force. This setup is realized when we control the external force f_{ext} so that the sliding velocity v may be constant. Then the frictional force f_{fric} can be considered as a function of the sliding velocity.

The traditional way of the statistical mechanics called the linear response theory appears to solve the problem if the velocity is much smaller than the rate ξ/τ, where ξ and τ are the characteristic length and time of the system, respectively. However, we already know well that the static frictional force is non-zero for several systems, for which the frictional force has a non-linear velocity dependence. This shows us the complexity of the problem which cannot be captured by applying the traditional way.

Several model calculations and experiments have solved these problems, directly or indirectly. Phononic contributions to sliding frictions were analyzed by the Frenkel-Kontorova model, whereas eletronic contributions were discovered and explained within an image potential theory. Furthermore as additional phenomena, sliding frictions between adsorbed Helium atoms and its substrates are recently getting attention, but their theoretical description is still not satisfactory and remains to an open problem.

Review the way of solving.

1.2 Impossibility of the Observation of the Sliding Surface

The dimensionality of the sliding surface is up to two, if that of the whole system is three. Sliding surfaces are different in many ways from the standard two-dimensional surfaces on three-dimensional solids which have been investigated for many years, so that we cannot perform a direct observation of the sliding surface by apparatuses such as microscopes. The difficulty prevents us from clarifying non-equilibrium properties of the sliding friction.

Solve the contradiction between the paragraph above and below.

There is a way to observe the sliding surface with the microscope and optically transparent matters, but most researches avoid a direct observations by measuring other observables to observe the sliding surface indirectly.

1.3 Manipulating the Friction

Recent researches well revealed the nature of sliding frictions. This gave rise to new problems about the friction in atomically microscopic systems.

Ordinary frictions in solids are mostly governed by excitations of phonon degrees of freedom, because the sliding surface is almost always rougher than the scale of the atom. Once we lubricate the sliding surface highly, other degrees of freedom such as the orbital and the spin angular momenta of electrons emerge as additional contributions to the friction.

We are already familiar with the most remarkable example of such a system in our daily lives, namely *micro electric mechanical systems* (**MEMS**). MEMS plays important roles in the printing head of inkjet printers, the accelerometer in smartphones and so on. MEMS has clean planes sliding with an accuracy of a micrometer or a nanometer, because of which they

experience a new type of the friction that ¡explanation¿. The small size of these systems makes the problem more serious, because the ratio of the surface area over the volume of the system become larger with the smaller size and a fixed geometry.

We have to tackle with the issue of manipulation the friction in such small systems by getting more fundamental knowledges of the friction.

1.4 Magnetic Friction

In this work we consider two strips of the quasi-one-dimensional Ising model sliding against each other with a fixed velocity. We discuss the difference of the frictional forces for the two boundary conditions, the anti-parallel and the parallel, and its dependence on the distance from one boundary to the other.

Based on the results in Ref. [2], we consider a dimensional crossover from one dimension to two in Ising models with two fixed boundary conditions. In the one-dimensional limit the boundary conditions seem to have the maximum effect on the friction, whereas in the two-dimensional limit there seems to be no effects. Behaviors in the both limits for the free boundary conditions correspond to the results in Ref. [2]. We find a method of manipulating the friction using different boundary conditions. These boundary conditions can be realized in experiments by aligning the boundary spins of sliding magnets.

The way to manipulate the friction in such small systems is less understood than its nature. We here consider manipulation of magnetic materials numerically simulating lattice models and their numerical simulations.

Frictions in such models were considered first in a numerical study by Kadau *et al.* [1]. They revealed by Monte Carlo simulations that two square lattices of the Ising model which slide against each other experience the friction, depending on the temperature and the sliding

velocity. Immediately after the research, it was revealed [2] that the Ising model goes under a non-trivial non-equilibrium phase transition (**NEPT**) in the high-velocity limit, where the two square lattices are decoupled in terms of the correlation between the two lattices and feel an effective mean field depending on the magnetization of each other [2]. This analysis showed that a novel critical point which is located at a generally higher temperature than the ordinal critical point for models in arbitrary dimensions and geometries (see Chapter 2). They also developed a new dynamics [2] which enables an analytical treatment for finite sliding velocities, obtaining the non-equilibrium critical line.

Chapter 2

Velocity-driven Non-equilibrium Phase Transition in Ising Models

To discuss the non-equilibrium crossover between two different dimensions, we have to make a brief review of the exact results [2] by Hucht. His analysis is based on the fact that two Ising cylinders with relative motion make a novel mean field and they lead the system to a non-trivial phase transition.

We now consider two equivalent square lattices of Ising model each of which contacts with the other by one of its one-dimensional boundary. If we leave two models alone, we can regard the models as an Ising model with a twice the size. With the coupling to the heat bath, we expect the model thermalize. But one of the couple are moving along the contact plane with a constant velocity v, the entire model goes into a non-equilibrium stationary state, instead of thermalization. The non-equilibrium stationary state well describes the behavior of two magnetic materials with a friction. This setup are explained in detail in Chapter 3.

As a well known fact, the ordinary two dimensional Ising model has the phase transition at the critical temperature $T_{\rm c} = 2/(\log\left[1+\sqrt{2}\right])$ in the thermodynamical limit $N/V \to \infty$,

N/V = const., where N is the number of spins and V is the volume of the system as a well known fact. The model with the friction becomes equivalent to the equilibrium case for the limit of $v \to 0$. The result [2] claims that the critical temperature T_c *branches* at the point $v = 0$ towards the limit $v = \infty$. Now we denote the velocity dependent non-equilibrium critical point by $T_c(v)$ apart from the equilibrium critical point $T_{eq,c}$. The system exhibits the ordinary phase transition and a novel phase transition where the magnetization grows up near the inner boundary rather than the rest (See Figure 2.1).

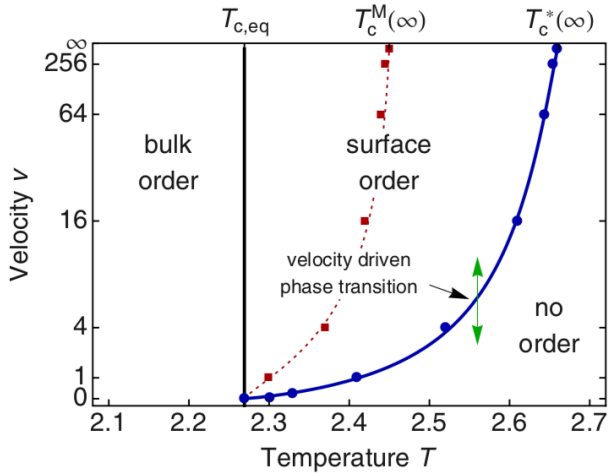

Figure 2.1: The phase diagram of the two-dimensional non-equilibrium Ising model. The black solid line, the blue solid line and the red dashed line indicate the ordinary bulk phase transition, a non-equilibrium boundary phase transition for the Multiplicative rate and the Metropolis rate respectively. From right to left across the non-equilibrium phase boundary the system acquires non-zero expectation value of magnetization on the inner boundary.

These phenomena were first reported in the numerical results [1] by Kadau et al. using Monte Carlo simulations both on the Metropolis rate and on the Glauber rate in a two-dimensional model, and then investigated in more analytic manner [2] by Hucht for several dimensions and model geometries. One of the important point in the latter result is that for the limit of $v \to 0$ we can write the closed exact equation for the *second* critical temperature $T_c(\infty)$. In addition it is also important that a novel algorithm, called *multipricative rate*, enabled us to give the equation of $T_c(v)$ which fully depends on the flip rate and the sliding

velocity $v > 0$.

If the velocity v is much less than the rate $\xi_x^{(\mathrm{eq})}(\beta)/\tau_x^{(\mathrm{eq})}(\beta)$, we can expect the system to behave well similarly to its equilibrium state, where $\xi_x^{(\mathrm{eq})}(\beta)$ and $\tau_x^{(\mathrm{eq})}(\beta)$ are the correlation length along the direction parallel to the sliding surface and the correlation time respectively for the equilibrium state of an inverse temperature $\beta := (k_{\mathrm{B}}T)^{-1}$. This corresponds to the case that the pumped energy by the constant sliding is most quickly relaxed towards the heat bath and the structure of domain walls near the inner boundary is well sustained. On the other hand, the velocity v much greater than the rate $\xi_x^{(\mathrm{eq})}(\beta)/\tau_x^{(\mathrm{eq})}(\beta)$ will lead the system to a stationary state much far from equilibrium so that the structure near the inner boundary will be destroyed.

In the latter case a mean field picture well describes the behavior of the system, where two sets of the moving spins along the contact plane act on the other *relatively* moving spins as the spatially-averaged effective field. In other words, the magnetization of one half of the system corresponds the effective field of the other, and vice versa. This enables us to write a self-consistent equation for the temperature $T_{\mathrm{c}}(\infty)$.

We summarize the result for one-dimensional chains and that of two-dimensional planes, in order to discuss the crossover from one-dimension to two-dimension in our models in Chapter 5.

We first give a general Hamiltonian of the Ising model as follows.

$$\beta\mathcal{H}_\mu := -\sum_{i<j} K_{ij}\sigma_i\sigma_j - \sum_i (h_i^{\mathrm{ext}} + k_i\mu_i)\sigma_i, \tag{2.1}$$

where K_{ij}, h_i^{ext} and $k_i\mu_i$ denotes the interaction between the i-th spin and the j-th one, the static field on the i-th spin and the stochastic field on the i-th spin ($\mu_i = \pm 1$) respectively. Now we

assume that μ_i obeys the probability distribution $p_i(\mu_i)$ such that $\langle \mu_i \rangle := \sum_{\mu_i=\pm 1} p_i(\mu_i)\mu_i = m_i$ for a given m_i. The form $p_i(\mu_i) := (1 + \mu_i m_i)/2$ actually satisfies the condition.

If we decompose the Hamiltonian into the contribution of the stochastic field and the rest one ($\beta\mathcal{H}_0 := -\sum_{i<j} K_{ij}\sigma_i\sigma_j - \sum_i h_i^{\rm ext}\sigma_i$) as

$$\beta\mathcal{H}_\mu = \beta\mathcal{H}_0 - \sum_i k_i\mu_i\sigma_i, \tag{2.2}$$

the partition function of the system is written as

$$\mathcal{Z} = {\rm Tr}_{\sigma\mu}\left[{\rm e}^{-\beta\mathcal{H}_\mu}\right] = {\rm Tr}_\sigma\left[{\rm e}^{-\beta\mathcal{H}_0}{\rm Tr}_\mu\left[\prod_i {\rm e}^{k_i\mu_i\sigma_i}\right]\right] = \prod_i \cosh k_i {\rm Tr}_\sigma\left[{\rm e}^{-\beta\mathcal{H}_0}\prod_i(1+\sigma_i m_i \tanh k_i)\right]. \tag{2.3}$$

On the other hand, if we give again a model with $k_i = 0$ as

$$\beta\mathcal{H}_{\rm eq} := -\sum_{i<j} K_{ij}\sigma_i\sigma_j - \sum_i h_i\sigma_i \tag{2.4}$$

which relaxes toward the well known equilibrium state, it holds that $\beta\mathcal{H}_{\rm eq} = \beta\mathcal{H}_0 - \sum_i b_i\sigma_i$ ($b_i := h_i - h_i^{\rm ext}$) and its partition function are written as

$$\mathcal{Z}_{\rm eq} = {\rm Tr}_\sigma\left[{\rm e}^{-\beta\mathcal{H}_{\rm eq}}\right] = {\rm Tr}_\sigma\left[{\rm e}^{\beta\mathcal{H}_0}\sum_i {\rm e}^{b_i\sigma_i}\right] \tag{2.5}$$

$$= \prod_i \cosh b_i {\rm Tr}_\sigma\left[{\rm e}^{-\beta\mathcal{H}_0}\prod_i(1+\sigma_i\tanh b_i)\right]. \tag{2.6}$$

Comparing right hand sides of (2.6) and (2.3), we have

$$\mathcal{Z} = \prod_i \frac{\cosh k_i}{\cosh b_i}\mathcal{Z}_{\rm eq} \tag{2.7}$$

under the condition $\tanh b_i = m_i \tanh k_i$.

We consider the model with the condition $h_i^{\rm ext} = 0$. Due to the translation invariance along the sliding direction, we have the homogeneous boundary magnetization $m_i = m_{\rm b}$ for all sites $\{i\}$. It results in the self-consistency that each boundary magnetization on the two internal-boundary lines act on each other as an effective field, and it holds that $h_i = h_{\rm b}$ for an existing $h_{\rm b}$ and all i. Substituting them into the condition $\tanh b_i = m_i \tanh k_i$, we have

$$h_{\rm b} = \tanh^{-1}[m_{\rm b} \tanh K_{\rm b}]. \tag{2.8}$$

The boundary magnetization under a static field $h_{\rm b}$, in general, have a form of

$$m_{\rm b,eq}[K, h_{\rm b}] := \frac{\partial}{\partial h_{\rm eq}} \log \left[\mathcal{Z}_{\rm eq}\right], \tag{2.9}$$

and thus we have

$$m_{\rm b,eq}[K, \tanh^{-1}\left[m_b \tanh K_b\right]] = m_b \tag{2.10}$$

as a self-consistent relation for m_b.

As the well known relation, it holds that for the critical point

$$1 = \left.\frac{\partial m_{\rm b,eq}}{\partial m_{\rm b}}\right|_{m_{\rm b}=0}. \tag{2.11}$$

Expanding the left hand side of (2.11) to the first order of $m_{\rm b}$ around the $m_{\rm b} = 0$, we have

$$m_{\rm b,eq}[K, \tanh^{-1}\left[0\right] + m_b \tanh\left[K_{\rm b}\right] \left.\frac{\partial m_{\rm b,eq}}{\partial h_{\rm b}}\right|_{h_{\rm b}=0} = m_b \tag{2.12}$$

and thus with the definition of the susceptibility at an equilibrium $\chi^{(0)}_{\mathrm{b,eq}}(K) := \partial m_{\mathrm{b,eq}}/\partial h_{\mathrm{b}}|_{h_{\mathrm{b}}=0}$ and the fact $m_{\mathrm{b,eq}}\left[K, \tanh^{-1}[0]\right] = 0$, we finally have

$$\tanh\left[K_{\mathrm{b}}\right]\chi^{(0)}_{\mathrm{b,eq}}(K) = 1 \tag{2.13}$$

for the critical condition. The condition (2.10) or (2.13) determines the non-equilibrium critical temperature for the limit $v \to \infty$. Using the expression of the magnetization for one-dimensional model and the boudnary magnetization for two-dimensional model, we have the numerical solution of the condition

$$T_{\mathrm{c},d=2} = 2.2691853\ldots \tag{2.14}$$

$$T_{\mathrm{c},d=3} = 2.6614725\ldots \tag{2.15}$$

respectively for the isotropic case $K = K_{\mathrm{b}}$.

Chapter 3

Numerical Simulations

3.1 Setup of the Model

Sliding friction is a form of energy dissipation on the surface between a moving object and its substrate. The dissipated energy is originated in the kinetic energy of the moving object. We here consider constantly moving case in which an external force maintains the motion of the object with endless supply of its kinetic energy. This view leads to its *non-equilibrium stationary state*. When the system is in a non-equilibrium stationary state, it is often easy to calculate several *energy currents* such as the frictional heat, its power and so on. Applying the view to our case where two square lattices of the Ising model slide against each other, we can formulate the problem as follows.

1. We prepare a square lattice of the Ising model of size $L_x \times L_z$ and impose periodic boundary conditions in the transverse (x) direction. We first set the system in the equilibrium state of a temperature T, whereas we set the open boundary conditions in the longitudinal (z) direction for the moment (see Figure 3.1a).

2. We cut the system along the x-direction into two parts, maintaining interactions on the

cut (see Figure 3.1b).

3. We slide two parts along the cut plane with relative velocity v. In other words, we shift the upper half by a lattice constant every $1/v$ unit time.

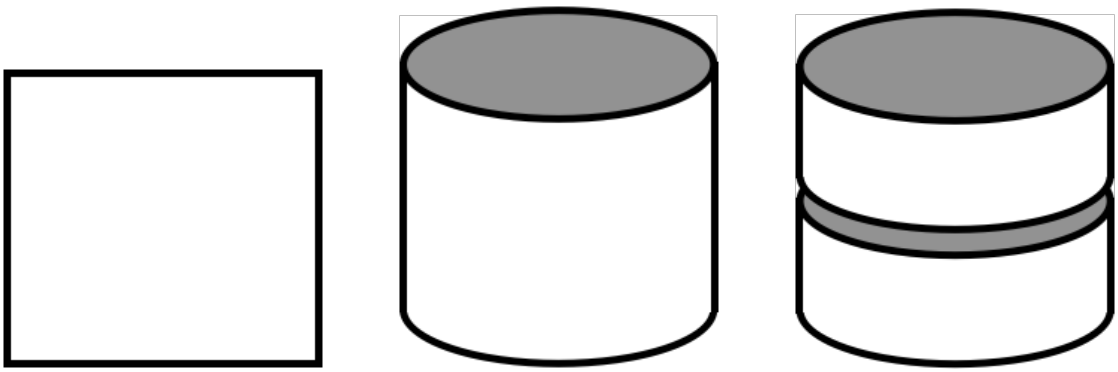

(a) A planar Ising model (b) A cylindrical Ising model (c) A cut Ising model

The Hamiltonian of the system is given by

$$\hat{H} = \hat{H}_{\text{upper}} + \hat{H}_{\text{lower}} + \hat{H}_{\text{slip}}(t), \tag{3.1}$$

where

$$\hat{H}_{\text{upper}} := -J \sum_{\langle i,j \rangle \in \text{upper}} \hat{\sigma}_i \hat{\sigma}_j, \tag{3.2}$$

$$\hat{H}_{\text{lower}} := -J \sum_{\langle i,j \rangle \in \text{lower}} \hat{\sigma}_i \hat{\sigma}_j, \tag{3.3}$$

$$\hat{H}_{\text{slip}}(t) := -J \sum_{\langle i,j(t) \rangle \in \text{slip}} \hat{\sigma}_i \hat{\sigma}_{j(t)}, \tag{3.4}$$

where *upper*, *lower* and *slip* represent the set of interacting spin pairs the upper half, the lower half and the slip plane of the entire system. Shift operations lead the system to repeated *pumping* and *dissipation* processes as follows:

1. **Shifting**: A shift operation excites the energy on the slip plane by the ammount $\langle \hat{H}_{\text{slip}}(t') -$

$\hat{H}_{\rm slip}(t)\rangle_{\rm st}$. The letter t' denotes the time just after the shift operation from the time t.

2. **Relaxing-1**: The excited energy on the slip plane dispenses to the entire system $\langle \hat{H}_{\rm upper} + \hat{H}_{\rm lower} + \hat{H}_{\rm slip}(t)\rangle_{\rm st}$.

3. **Relaxing-2**: The excited entire system relaxes toward the equilibrium the heat bath.

We defined the stationary state average $\langle \hat{A} \rangle_{\rm st} := \sum_i A_i p_i^{\rm (st)}$ for an arbitrary observable $\hat{A}$, where $\{A\}_i$ are eigenvalues of $\hat{A}$ and $\{p_i^{\rm (st)}\}$ are stationary state probability distribution. Note that the distribution $\{p_i^{\rm (st)}\}$ are quite different from the equilibrium (canonical) probability distribution $p_i^{\rm (eq)} \propto \exp\left[-E_i/k_{\rm B}T\right]$. In addition, the distribution $\{p_i^{\rm (st)}\}$ depends on the sliding velocity v, and therefore it has infinite number of families.

The excited and relaxed amounts of energy per unit time correspond to the energy pumping and dissipation, respectively. The energy pumping $P(t)$ and dissipation $D(t)$ are given by

$$P(t) := \sum_{i_v=0}^{v-1} \left\langle \hat{H}_{\rm slip}\left(t' - 1 + \frac{i_v}{v}\right) - \hat{H}_{\rm slip}\left(t - 1 + \frac{i_v}{v}\right) \right\rangle_{\rm st}, \tag{3.5}$$

$$D(t) := \sum_{i_v=0}^{v-1} \left\langle \hat{H}_{\rm slip}\left(t - 1 + \frac{i_v + 1}{v}\right) - \hat{H}_{\rm slip}\left(t' - 1 + \frac{i_v}{v}\right) \right\rangle_{\rm st}. \tag{3.6}$$

3.2 Definitions of Physical Quantities

We now consider the case in which that the system is in a non-equilibrium stationary state. We define the frictional force density $f(L_z, T)$ by

$$f(L_z, T) := \lim_{L_x \to \infty} \frac{F(L_x, L_z, T)}{L_x}, \tag{3.7}$$

where $F(L_x, L_z, T)$ is the frictional force of a system of size $L_x \times L_z$ at a temperature T. We numerically formulate the large-size limit $L_x \to \infty$ as follows.

Numerical large-size limit $L_x \to \infty$

If the quantity $F(L_x, L_z, T)/L_x$ is independent on L_x, $F(L_x, L_z, T)/L_x$ is a good approximation for $f(L_z, T)$.

In numerical simulations, we calculate the frictional force $F(L_x, L_z, T)$ using its power $D(L_x, L_z, T)$ by the formula

$$F(L_x, L_z, T) = \frac{D(L_x, L_z, T)}{v}, \tag{3.8}$$

where the quantity $D(L_x, L_z, T)$ is the long-time limit of $D(t)$ for the lattice of $L_x \times L_z$ at a temperature T.

We can easily verify the formula (3.8) by considering general cases in which the frictional force and its power are both time dependent. Denoting the frictional force $F(x)$ at the position x, it holds that

$$\int_{t_0}^{t_1} dt\ D(t) = \int_{x(t_0)}^{x(t_1)} dx\ F(x) = \int_{t_0}^{t_1} \frac{dx}{dt} dt\ F(x(t)) = v \int_{t_0}^{t_1} dt\ F(x(t)), \tag{3.9}$$

for a time dependent $D(t)$, because $dx/dt = v$. Under the assumption of a non-equilibrium stationary state, in the long-time limit, the integrands in both hand sides of the relation (3.9) are still equal to each other, and hence

$$D(L_x, L_z, T) = vF(L_x, L_z, T). \tag{3.10}$$

From now we call the quantity $D(L_x, L_z, T)$ *energy dissipation*.

Our models always reach non-equilibrium stationary states in the long-time limit $t \to \infty$, which depend on the temperature T and the sliding velocity v; We will prove in App. A. We

use the fact that $\lim_{t\to\infty}|D(t)| = \lim_{t\to\infty}|P(t)|$ in order to calculate average value $\bar{D}$ with less fluctuation by using the value $\bar{P}$ [3–5]. We therefore have

$$P(L_x, L_z, T) = vF(L_x, L_z, T). \tag{3.11}$$

We also define the bulk energy density $\epsilon_{\rm b}(L_z, T)$ as follows

$$\epsilon_{\rm b}(L_z, T) := \lim_{L_x\to\infty} \frac{E_{\rm b}(L_x, L_z, T)}{L_x L_z}, \tag{3.12}$$

where $E_{\rm b}(L_x, L_z, T)$ is the energy of entire system. Straightforwardly, we define the bulk heat capacity $c_{\rm b}(L_z, T)$ as follows

$$c_{\rm b}(L_z, T) := \frac{\partial \epsilon_{\rm b}(L_z, T)}{\partial T}. \tag{3.13}$$

3.3 Non-equilibrium Monte Carlo Simulation

Energy dissipation process towards the heat bath occurs via a spin flip. This fundamental processes do not only describe equilibrium states, but also non-equilibrium stationary states for a fixed temperature T [6]. Using Monte Carlo method, we can simulate this process.

3.3.1 Introduction the Time Scale to Ising Models

The Ising model which we deal with is a kind of kinetic Ising models [6], in which its time dependent statistics plays several important roles. In order to calculate dynamical observables such as the frictional power (3.11) and its dissipation rate (3.8), we have to define *a unit time* for finite size systems. We now consider the case in which a homogeneous spin chain of

the volume L and a heat bath with the temperature T are interacting. This system are well described with enough large number of the spins. Denoting such a number N, we can consider two macroscopically equivalent models as follows:

- An N-spin chain with the lattice constant $a = L/N$,
- An $(M \times N)$-spin chain with the lattice constant $a = L/(M \times N)$,

where M is the large number which have the same property as N. Since both of models well describe the system of volume L, typical time scale[1] of each system should be the same. And under the *homogeneousness* assumption that for both models each spin is independently interacting with the heat bath, the dynamics of any spin in the former and that of any M-spins subsystem in the latter are effectively equivalent. Thus as long as we consider the dynamics of same volume systems, we can define the unit time scale using its number of spins. This concept can be easily implemented on the ordinary *equilibrium* Monte Carlo simulation for classical spin systems.

For the equilibrium Monte Carlo simulation, the most naive approach for the equilibrium state is the single flip algorithm, where we perform the sequence a random selection of the spin and its flipping with temperature dependent probability $p(T)$. We often use the Metropolis probability $p_{\mathrm{M}}(T) := \min\{1, \mathrm{e}^{-\frac{\Delta E}{k_{\mathrm{B}}T}}\}$ as the probability $p(T)$, where ΔE is the energy difference by the flipping. The Metropolis probability $p_{\mathrm{M}}(T)$ have a good property, called *detailed balanced condition*, which certainly leads the system towards the true equilibrium state with enough many repetition of the algorithm. This process and randomness well describes the interaction and the homogeneousness with the heat bath. We often call *Monte Carlo step* a single process of the algorithm, and define *Monte Carlo sweep* N-times process, where N is the number of

[1] If we use the same criterion, any time scale may be introduced. For example, we can define *a typical time scale* as the time taken to flip all the spin.

spins. According to the earlier discussion, the unit time in the system is nothing but the Monte Carlo sweep. Thus the more spins the system contains, the higher time resolution we can simulate with.

3.3.2 Slip Plane with the Velocity v

Using the introduced time scale, we can also introduce the slip plane with the velocity v to the system with N-spins. Corresponding to the setup in Sec. 3.1, we perform the extended single flip algorithm as follows:

1. **Shifting**: We shift the upper half by a lattice constant.

2. **Flipping**: We perform ordinary single flips for N/v times.

3. We repeat the process 1 + 2 for $(v-1)$ times.

In the extended algorithm, the upper half slides with the velocity v in a unit time at regular intervals. We proved the fact that this algorithm lead the system of any size to the non-equilibrium stationary state depending the temperature T and the velocity v (see appendix A in detail).

3.3.3 Calculation Method

The observables which we are interested in are the frictional power $P(t)$ and its dissipation rate $D(t)$. In Monte Carlo simulations, the frictional power $P(t)$ and the dissipation rate $D(t)$ are the energy difference by the shifting operation and that by the flipping respectively, for a unit time. Both observables have the same absolute value in the long time limit.

Chapter 4

Results of Simulations

In this chapter, we show the results of Monte Carlo simulations of the Ising models. To discuss the dependence of the frictional force density $f(L_z, T)$ and the bulk energy density $\epsilon_{\rm b}(L_z, T)$ on the size L_z and the temperature T with the fixed velocity $v = 10$, we performed the numerical large size limit $L_x \to \infty$ with the fixed L_z and T (see appendix B.1). To get the observables in the non-equilibrium stationary state, we performed the equilibration process for 5000 sweeps and the stationarization process for 5000 sweeps for all given parameters. The convergence of the observables to the equilibrium value and the stationary value for these time regions respectively are checked carefully.

The range of parameters in our simulation is as follows. We computed the value of $f(L_z, T)$ for temperatures $k_{\rm B}T/J \in \{0.0, 0.1, 0.2, \ldots, 1.9, 2.0, 2.02, 2.04, \ldots, 2.48, 2.50, 2.6, 2.7, \ldots, 5.0\}$ and sizes $L_z \in \{4, 6, 8, 10, 12, 14, 16, 32, 64\}$ with the two boundary conditions, the anti-parallel and the parallel. For the anti-parallel boundary the initial state is set to the domain-wall state, where spin variables σ_i in the upper half of the system are the same value as the upper boundary, and in the lower half as the lower boundary. For the parallel boundary the initial state is set to the magnetized state, where all spin variables σ_i are the same value as both

of boundaries. The reason why we used these initial states is that they are the most natural ground states which correpond to each of the boundary conditions.

All the simulations are performed by the single flip algorithm with the Metropolis rate. We performed these simulations for 480 samples for all parameters and averaged them, and then averaged along the time direction.

In addition, we also show their temperature derivatives to discuss the phase transitions.

4.1 Frictional Force Density $f(L_z, T)$

We show the behavior of the frictional force density $f(L_z, T)$ (see Figure 4.1). For both boundary conditions, the anti-parallel and the parallel, extremely smaller sizes such as $L_z = 4, 6$ make greater differences from its value for the current maximum size $L_z = 64$, where an asymptotic behavior emerges. We can expect that for more larger sizes such as $L_z = 128, 256, \ldots$ makes no longer great differences from that of $L_z = 64$, thus we can say that the system reaches *two-dimension* in the vicinity of the size $L_z = 16$.

An additional important aspect is the difference between the values for anti-parallel and the parallel boundary conditions. In the former case, the smaller size L_z makes the greater value of the frictional force density $f(L_z, T)$. On the other hand, the latter case indicates the reverse behavior that smaller size L_z makes the smaller value of the frictional force density $f(L_z, T)$. This physical meaning is that the size L_z and the correlation length of the system along the z-direction $\xi_z(\beta)$ become comparable, and then the system behaves as the one-dimension for the smaller size L_z, whereas much greater size L_z than the correlation length $\xi_z(\beta)$ makes the system two-dimensional. Note that for $L_z = 64$ behaviors for both cases are similar to each other and we can expect that these behaviors reach to the results by Kadau [1].

We additionally show the behavior of its temperature derivative $\partial f(L_z, T)/\partial T$ (see Figure

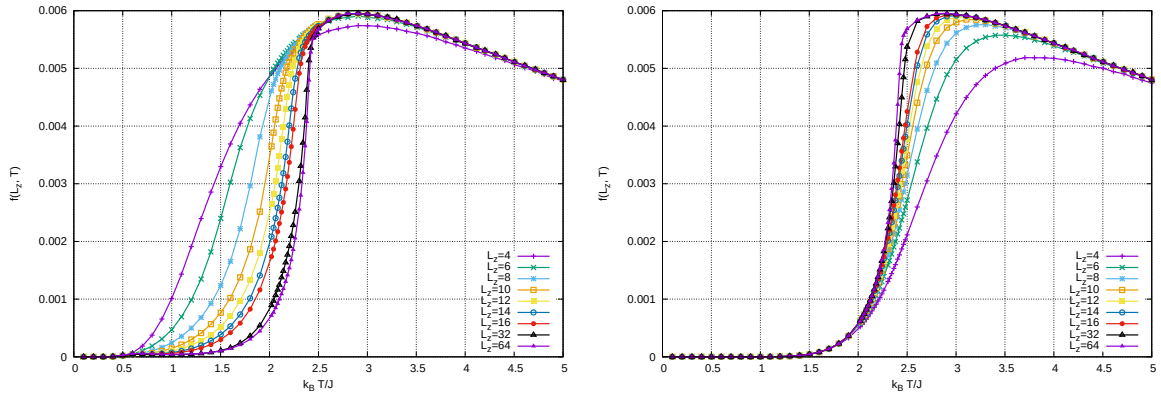

(a) Anti-parallel boundary condition (b) Parallel boundary condition

Figure 4.1: The temperature T dependence of the frictional force density $f(L_z, T)$ with the parallel boundary condition along the z-direction for each longitudinal size L_z are plotted.

4.2). These exhibits the crossover-driven divergence at characteristic temperatures, near $T = 2.40$ for both boundary conditions to reflect the steeper slopes of the frictional force density $f(L_z, T)$. If we regards the peak $T_{\rm peak}(L_z)$ as the pseudo critical point for all sizes $L_z = 4, 6, 8, 10, 12, 14, 16, 32, 64$, where $\partial^2 f(L_z, T)/\partial T^2|_{T=T_{\rm peak}(L_z)} = 0$, we can recognize the shift of peaks toward the higher temperature for the anti-parallel boundary, whereas peaks shifts toward the lower for the parallel boundary. These describes the effects of the boundary condition which acts on the system as an effective field, and the effects are enhanced by the smaller L_z. Namely the anti-parallel boundary acts as a demagnetizing field such that the pseudo critical point $T_{\rm peak}(L_z)$ shifts toward the lower, and the parallel boundary acts as a magnetizing field such that the pseudo critical point $T_{\rm peak}(L_z)$ shifts toward the higher.

Remarkably peaks $\{T_{\rm peak}(L_z)\}$ for both boundaries hit the temperature higher than the ordinary critical point $T_{\rm c} = 2/\log\left[1+\sqrt{2}\right]$. This implies that both the ordinary phase transition and the non-equilibrium phase transition occur at two different temperatures.

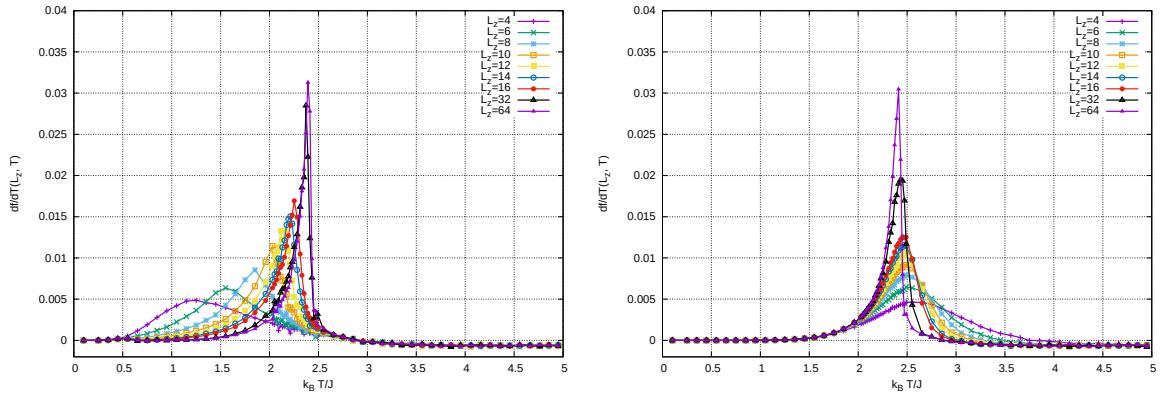

(a) Anti-parallel boundary condition (b) Parallel boundary condition

Figure 4.2: The temperature T dependence of the temperature derivative $\partial f(L_z, T)/\partial T$ with the parallel boundary condition along the z-direction for each longitudinal size L_z are plotted.

4.2 Bulk Energy Density $\epsilon_{\rm b}(L_z, T)$

We show the behavior of the bulk energy density $\epsilon_{\rm b}(L_z, T)$ (see Figure 4.3). As same as frictional force densities $f(L_z, T)$, bulk energy densities $\epsilon_{\rm b}(L_z, T)$ indicates an asymtotic behavior.

In the anti-parallel case, the smaller size L_z makes the system well disorder. On the other hand, the parallel case indicates no drastic change driven by the smaller size L_z.

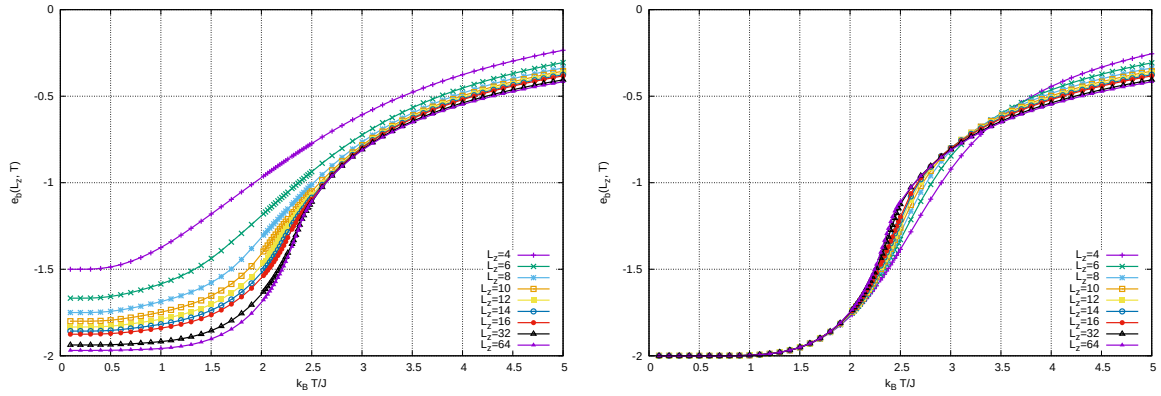

(a) Anti-parallel boundary condition (b) Parallel boundary condition

Figure 4.3: The temperature T dependence of the bulk energy density $\epsilon_{\rm b}(L_z, T)$ with the parallel boundary condition along the z-direction for each longitudinal size L_z are plotted.

We additionally show the behavior of the heat capacity $c_{\rm b}(L_z, T) = \partial \epsilon_{\rm b}(L_z, T)/\partial T$ as its temperature derivative (see Figure 4.2). The behavior is similar to that of the temperature derivative of the frictional force density $\partial f(L_z, T)/\partial T$ in terms of the peak $T_{\rm peak}(L_z)$ for enough

larger sizes.

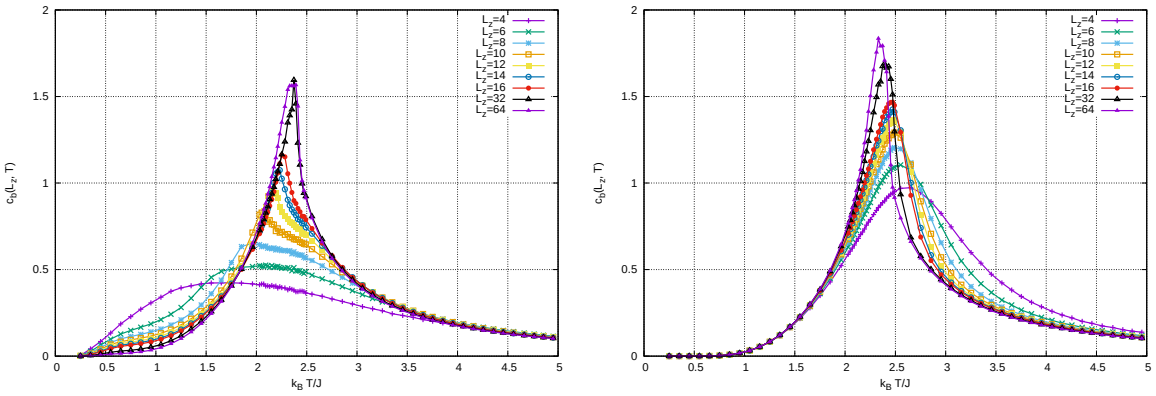

(a) Anti-parallel boundary condition

(b) Parallel boundary condition

Figure 4.4: The temperature T dependence of the bulk energy density $\epsilon(L_z, T)$ with the parallel boundary condition along the z-direction for each longitudinal size L_z are plotted.

Chapter 5

Summary and Discussion

In this paper, we considered fixing the boundary condition on the two boundary planes parallel to the slip plane as manipulating the magnetic friction in two-dimensional systems and investigated the effects of fixing variations on the magnetic friction by changing the distance L_z between the two boundary planes. As the result, we discovered that two scales of length, the distance L_z and the correlation length ξ_z, makes a dimensional crossover from one-dimension to two-dimension. We also saw that peaks of the derivatives, $\partial f(L_z, T)/\partial T$ and $\partial \epsilon_{\mathrm{b}}/\partial T$, for cases of size $L_z = 4$ and $L_z = 64$, and both of them imply the non-equilibrium phase transition reported by Hucht [2] and the locations of peaks are consistent to their results for the case $v = 10$.

For future works, we are going to investigate

- Consistency between the case of free boundary condition to the results by Hucht [2]
- Divergence of derivatives of the *boundary* energy (or boundary capacity) for the limit of two-dimension
- Behavior of the correlation length itself

- Dimensional crossover of the critical exponents of $\partial f(L_z, T)/\partial T$ and $\partial \epsilon_{\mathrm{b}}/\partial T$

to analyze the phenomena in more detail. We intend to see whether dimensional crossovers in models with other spatial dimensions or continuous symmetries.

Appendix A

Analysis based on Stochastic Matrices

In this chapter, we prove the existence of the non-equilibrium stationary state in our model with a half sliding for arbitrary velocities $v > 0$. In the first section, we discuss the formulation by stochastic matrices, and then see Monte Carlo simulations and the stochastic matrices are equivalent in terms of the probability with a simple example. In the following two sections, we prove several facts for stochastic matrices, which ensures that almost all Monte Carlo simulations converge to a equilibrium state and its uniqueness, and then the properties are taken over and lead to a unique stationary state even if the matrix contains a kind of perturbation factors. In the last two sections, we propose the way to construct the matrix for both equilibrium cases and non-equilibrium stationary cases, and discuss the distributions of their eigenvalues in terms of the convergence.

A.1 A Simple Example: Stochastic Ising Model with N-spins

Monte Carlo simulations for lattice spin systems extract the relevant subspace from the full space instead of an exact calculation of the partition function using a stochastic process. The subspace depends on given parameters and if we use the canonical distribution with a fixed temperature T, the temperature determines the subspace. The stochastic process is expressed as a trajectory of variables by the time in the subspace. Averaging the trajectory for an enough long time, we can compute physical quantities with any desired accuracy.

We now consider a matrix form of the stochastic process. For example, the one-dimensional Ising chain with N-spins has 2^N states. If we labeled each of the states by $i = 1, 2, \ldots, 2^N$, we can write the stochastic time evolution of the system by a set of the existence probabilities $\{p_i(t)\}$ such that the system is in the i-th state at a time t, and the transition probabilities T_{ij} such that the system in the j-th state changes to the i-th state. Note that not the transition probabilities T_{ij} but the existence probabilities $\{p_i(t)\}$ play the role of time evolution.

We additionally define the conditional probability $\tilde{p}_{ij}(t)$ such that the system in the j-th state at a time t changes to the i-th state at the next time $t + 1$. Using the conditional probability, we can derive the relation between the existence probability $p_i(t)$ and the transition probability T_{ij} as

$$\tilde{p}_{ij}(t+1) = T_{ij} p_j(t) \quad \text{for } 1 \leq i, j \leq 2^N. \tag{A.1}$$

From a property as the probability, it should hold that $\sum_{i=1}^{2^N} p_i(t) = 1$ and $p_i(t) \geq 0$ ($i = 1, 2, \ldots, 2^N, t \in \mathbb{R}$). The conditional probability $\tilde{p}_{ij}(t)$ should also satisfy the condition that

$\sum_{j=1}^{2^N} \tilde{p}_{ij}(t) = p_i(t+1)$ $(i = 1, 2, \ldots, 2^N, t \in \mathbb{R})$. Then we have

$$p_i(t+1) = \sum_{j=1}^{2^N} \tilde{p}_{ij}(t+1) = \sum_{j=1}^{2^N} T_{ij} p_j(t) \quad \text{for } 1 \leq i \leq 2^N,\ t \in \mathbb{R}. \tag{A.2}$$

In the other words, the system can be described by the probability vector $\boldsymbol{p}(t) := {}^{\mathrm{t}}(p_1(t), p_2(t), \ldots, p_{2^N}(t))$ and the stochastic matrix $\hat{T} := (T_{ij})$ as

$$\boldsymbol{p}(t+1) = \hat{T}\boldsymbol{p}(t) \quad \text{for } t \in \mathbb{R}. \tag{A.3}$$

In Monte Carlo simulations, we often trace the trajectory of a component of the vector $\boldsymbol{p}(t)$, thus we rarely need to construct the matrix $\hat{T}$. But it is helpful for us to consider such the matrix when we discuss the convergence to the stationary state or its uniqueness. These discussions are valid for general Ω-dimensional state spaces, thus we denote the number of states by Ω from now on.

A.2 General Theory of Stochastic Matrices

In this section we discuss the conditions which ensure a convergence of the corresponding Monte Carlo simulation to a unique stationary state. We first define the stochastic matrix and discuss fundamental properties of the stochastic matrix. We next discuss the properties which result from an additional condition called *weak/strong connectivity*, which leads the existence and the uniqueness of a stationary state. We also see that we can construct a stochastic matrix which leads to any desired stationary state under the so-called *detailed balanced condition*.

From the condition $\sum_{i=1}^{\Omega} p_i(t) = 1$ and $p_i(t) \geq 0$ $(i = 1, 2, \ldots, \Omega, t \in \mathbb{R})$, we have a set of properties $\sum_{i=1}^{\Omega} T_{ij} = 1$, $T_{ij} \geq 0$ $(1 \leq i \leq \Omega)$. Any matrix with these conditions is called

stochastic matrix and shows the following interesting property:

Theorem A.2.1. Let $\hat{T}$ be a stochastic matrix, then all absolute values of eigenvalue are less than or equal to 1. For any eigenvector $\boldsymbol{x} = {}^{\mathrm{t}}\{x_1, x_2, \ldots, x_\Omega\}$ which does *not* belong to the eigenvalue 1, it additionally holds that

$$\sum_{i=1}^{\Omega} x_j = 0. \tag{A.4}$$

We now define the vector $\boldsymbol{d} := {}^{\mathrm{t}}(1, 1, \ldots, 1)$ to prove all facts after this.

Proof. For any stochastic matrix $\hat{T}$, we have

$$\left({}^{\mathrm{t}}\hat{T}\boldsymbol{d}\right)_i = \sum_{j=1}^{\Omega} \left({}^{t}T\right)_{ij} d_j = \sum_{j=1}^{\Omega} T_{ji} d_j = \sum_{j=1}^{\Omega} T_{ji} = 1 \quad \text{for } i = 1, 2, \ldots, \Omega, \tag{A.5}$$

$$\iff \quad {}^{\mathrm{t}}\hat{T}\boldsymbol{d} = \boldsymbol{d}. \tag{A.6}$$

Therefore the matrix ${}^{\mathrm{t}}\hat{T}$ has an eigenvalue 1 at least. The eigenequation for the matrix ${}^{\mathrm{t}}\hat{T}$ are rewritten as

$$\det\left[\lambda\hat{I}_\Omega - {}^{\mathrm{t}}\hat{T}\right] = \det\left[{}^{\mathrm{t}}\left(\lambda\hat{I}_\Omega - \hat{T}\right)\right] = \det\left[\lambda\hat{I}_\Omega - \hat{T}\right], \tag{A.7}$$

and then the set of eigenvalues of $\hat{T}$ is equal to that of ${}^{\mathrm{t}}\hat{T}$. Finally the matrix $\hat{T}$ has an eigenvalue 1 at least. A general eigenvalue equation of $\hat{T}$ can be written as

$$\hat{T}\boldsymbol{x}_\lambda = \lambda\boldsymbol{x}_\lambda, \tag{A.8}$$

where $\boldsymbol{x}_\lambda = {}^{\mathrm{t}}(x_{\lambda,1}, x_{\lambda,2}, \ldots, x_{\lambda,\Omega})$ is its eigenvector. We have

$$((l.h.s \text{ of A.8}), \boldsymbol{d}) = (\hat{T}\boldsymbol{x}_\lambda, \boldsymbol{d}) = (\boldsymbol{x}_\lambda, {}^{\mathrm{t}}\hat{T}\boldsymbol{d}) = (\boldsymbol{x}_\lambda, \boldsymbol{d}), \tag{A.9}$$

$$((r.h.s \text{ of A.8}), \boldsymbol{d}) = (\lambda\boldsymbol{x}_\lambda, \boldsymbol{d}) = \lambda(\boldsymbol{x}_\lambda, \boldsymbol{d}). \tag{A.10}$$

$$\iff \quad (1-\lambda)(\boldsymbol{x}_\lambda, \boldsymbol{d}) = 0 \quad \iff \quad \lambda = 1 \text{ or } (\boldsymbol{x}_\lambda, \boldsymbol{d}) = 0. \tag{A.11}$$

$$\iff \quad \sum_{i=1}^{\Omega} x_{\lambda,i} = 0 \quad \text{if } \lambda \neq 1. \tag{A.12}$$

We additionally define the vector $\boldsymbol{y}_\lambda := {}^{\mathrm{t}}(|x_{\lambda,1}|, |x_{\lambda,2}|, \ldots, |x_{\lambda,\Omega}|)$ for any λ. From the equation $\sum_{j=1}^{\Omega} T_{ij}x_{\lambda,j} = \lambda x_i (i = 1, 2, \ldots, \Omega)$ we have

$$|\sum_{j=1}^{\Omega} T_{ij}x_{\lambda,j}| \leq \sum_{j=1}^{\Omega} T_{ij}|x_{\lambda,j}| \quad (\because T_{ij} \geq 0 \quad \text{for } j = 1, 2, \ldots, \Omega) \tag{A.13}$$

$$= \left(\hat{T}\boldsymbol{y}_\lambda\right)_i \quad \text{for } i = 1, 2, \ldots, \Omega. \tag{A.14}$$

and the left hand side of (A.14) are rewritten as

$$|\sum_{j=1}^{\Omega} T_{ij}x_{\lambda,j}| = |\lambda x_{\lambda,j}| = |\lambda| \times |x_{\lambda,j}| = |\lambda| \times (\boldsymbol{y}_\lambda)_j\,, \tag{A.15}$$

thus we have

$$|\lambda| \times (\boldsymbol{y}_\lambda)_j \leq \left(\hat{T}\boldsymbol{y}_\lambda\right)_i\,, \tag{A.16}$$

$$\iff \quad |\lambda| \times (\boldsymbol{y}_\lambda, \boldsymbol{d}) \leq \left(\hat{T}\boldsymbol{y}_\lambda, \boldsymbol{d}\right) = \left(\boldsymbol{y}_\lambda, {}^{\mathrm{t}}\hat{T}\boldsymbol{d}\right) = (\boldsymbol{y}_\lambda, \boldsymbol{d})\,, \tag{A.17}$$

$$\iff \quad |\lambda| \leq 1. \tag{A.18}$$

□

We limit the class of stochastic matrices to that of weakly connected ones from now on.

Definition A.2.1. For an arbitrary $1 \leq i, j \leq \Omega$, if there exists an $n(i,j) > 0$ such that

$$\left(\hat{T}^{n(i,j)}\right)_{ij} > 0, \tag{A.19}$$

the matrix $\hat{T}$ is called *weakly connected*. Note that for any $n' > n(i,j)$ it does *not* follows that $\left(\hat{T}^{n'}\right) > 0$.

To make proofs easier, we also define the matrix $\hat{\mathcal{T}}_\epsilon$ ($\epsilon > 0$) and discuss its properties. Denoting the maximum value of $n(i,j)$ by $n_{\max} := \max_{1 \leq i,j \leq \Omega} [n(i,j)]$ and defining the matrix $\hat{\mathcal{T}}_\epsilon := \left(\hat{I}_\Omega + \epsilon \hat{T}\right)^{n_{\max}}$, we have

$$\left(\hat{\mathcal{T}}_\epsilon\right)_{ij} = \left(\left(\hat{I}_\Omega + \epsilon \hat{T}\right)^{n_{\max}}\right)_{ij} = \sum_{k=1}^{n_{\max}} \binom{n_{\max}}{k} \left(\hat{I}_\Omega^k \left(\epsilon \hat{T}\right)^{n_{\max}-k}\right)_{ij} \tag{A.20}$$

$$= \sum_{k=1}^{n_{\max}} \binom{n_{\max}}{k} \epsilon^{n_{\max}-k} \left(\hat{T}^{n_{\max}-k}\right)_{ij} \geq 0 \quad (\because T_{ij} > 0) \quad \text{for } 1 \leq i, j \leq \Omega. \tag{A.21}$$

For the eigenvector $\boldsymbol{x}_1 = {}^{\mathrm{t}}(x_{1,1}, x_{1,2}, \ldots, x_{1,\Omega})$, which belongs to the eigenvalue 1, it holds that

$$\hat{\mathcal{T}}_\epsilon \boldsymbol{x}_1 = \sum_{k=1}^{n_{\max}} \binom{k}{n_{\max}} \epsilon^{n_{\max}-k} \hat{T}^{n_{\max}} \boldsymbol{x}_1 \tag{A.22}$$

$$= \sum_{k=1}^{n_{\max}} \binom{k}{n_{\max}} \epsilon^{n_{\max}-k} \boldsymbol{x}_1 \tag{A.23}$$

$$= (1+\epsilon)^{n_{\max}} \boldsymbol{x}_1, \tag{A.24}$$

and each component is

$$\sum_{j=1}^{\Omega} \left(\hat{\mathcal{T}}_\epsilon\right)_{ij} x_{1,j} = (1+\epsilon)^{n_{\max}} x_{1,i} \quad \text{for } i = 1, 2, \ldots, \Omega. \tag{A.25}$$

Theorem A.2.2. The phases of components of the vector $\boldsymbol{x}_1$ are aligned together and all the components are positive. In other words, we can decompose the vector into a phase factor and a positive vector as follows

$$\boldsymbol{x}_1 = \mathrm{e}^{i\theta} \boldsymbol{u}_1, \tag{A.26}$$

where θ is the phase and $\boldsymbol{u}_1$ is the vector with all positive component.

Proof. If components of the vector $\boldsymbol{x}_1$ are *not* aligned together such that $\sum_{i=1}^{\Omega} |x_{1,i}| > |\sum_{i=1}^{\Omega} x_{1,i}|$ holds, we have

$$|\sum_{j=1}^{\Omega} \left(\hat{\mathcal{T}}_\epsilon\right)_{ij} x_{1,j}| < \sum_{j=1}^{\Omega} \left(\hat{\mathcal{T}}_\epsilon\right)_{ij} |x_{1,j}| = (1+\epsilon)^{n_{\max}} |x_{1,i}|. \tag{A.27}$$

On the other hand, the row-wise sum of the matrix $\hat{\mathcal{T}}_\epsilon$ are

$$\sum_{i=1}^{\Omega} \left(\hat{\mathcal{T}}_\epsilon\right)_{ij} = \sum_{k=1}^{n_{\max}} \binom{k}{n_{\max}} \epsilon^{n_{\max}-k} \sum_{i=1}^{\Omega} \left(\hat{T}^{n_{\max}-k}\right)_{ij} = (1+\epsilon)^{n_{\max}}. \tag{A.28}$$

Then we have

$$\sum_{i=1}^{\Omega} \sum_{j=1}^{\Omega} \left(\hat{\mathcal{T}}_\epsilon\right)_{ij} |x_{1,j}| = (1+\epsilon)^{n_{\max}} \sum_{j=1}^{\Omega} |x_{1,j}| > (1+\epsilon)^{n_{\max}} \sum_{i=1}^{\Omega} |x_{1,i}|, \tag{A.29}$$

but it is the contradiction caused from our assumption $\sum_{i=1}^{\Omega} |x_{1,i}| > |\sum_{i=1}^{\Omega} x_{1,i}|$. Furthermore the left hand side of (A.25) is positive because that $n_{\max}$ is the maximum value of $n(i,j)$, and

then the right hand side is also positive. Then we have $x_{1,i} > 0 (i = 1, 2, \ldots, \Omega)$. □

Theorem A.2.3. The eigenspace of the matrix $\hat{\mathcal{T}}_\epsilon$, which belongs to the eigenvalue 1, is *one-dimensional*.

Proof. If we have two different eigenvectors, which belongs to the eigenvalue 1, we can write their eigenequations by two different *positive vectors* as

$$\hat{T}\boldsymbol{u}_1 = \boldsymbol{u}_1, \tag{A.30}$$

$$\hat{T}\boldsymbol{v}_1 = \boldsymbol{v}_1. \tag{A.31}$$

For their any linear superposition, we also have

$$\hat{T}(\boldsymbol{u}_1 + tv_1) = \boldsymbol{u}_1 + tv_1, \quad \text{for any } t \in \mathbb{R}. \tag{A.32}$$

But if two eigenvectors $\boldsymbol{u}_1$ and $\boldsymbol{v}_1$ are not aligned, we can make a non-trivial vector with a certain t such that $(\boldsymbol{u}_1 + tv_1)_l = 0$ for an l-th element. But it is the contradiction with the fact $x_{1,i} > 0 (i = 1, 2, \ldots, \Omega)$. Then we have no eigenspaces more than one, which belongs to the eigenvalue 1. □

We additionally limit the class of stochastic matrices to that of strongly connected ones from now on.

Definition A.2.2. If there exists a number $N_0 > 0$ such that

$$\left(\hat{T}^{N_0}\right)_{ij} > 0 \tag{A.33}$$

for an arbitrary $1 \leq i, j \leq \Omega$, the matrix $\hat{T}$ is called *strongly connected*.

Theorem A.2.4. There exists only the eigenvalue 1 with its absolute value 1.

Proof. We now have $\hat{T}^n \boldsymbol{u}_\lambda = \lambda^n \boldsymbol{u}_\lambda$, where $\boldsymbol{u}_\lambda = {}^{\mathrm{t}}(u_{\lambda,1}, u_{\lambda,2}, \ldots, u_{\lambda,\Omega})$ is the eigenvector which belongs to an eigenvalue λ. Their components are written as

$$\sum_{j=1}^{\Omega} \left(\hat{T}^n\right)_{ij} u_{\lambda,j} = \lambda^n \boldsymbol{u}_{\lambda,i}, \quad \text{for } i = 1, 2, \ldots, \Omega. \tag{A.34}$$

We can divide conditions for λ into following two cases:

Case1: $\sum_{i=1}^{\Omega} |u_{\lambda,i}| > |\sum_{i=1}^{\Omega} u_{\lambda,i}|$**,**

We have

$$\sum_{j=1}^{\Omega} \left(\hat{T}^n\right)_{ij} |u_{\lambda,j}| > |\sum_{j=1}^{\Omega} \left(\hat{T}^n\right)_{ij} u_{\lambda,j}| = |\lambda^n| \times |u_{\lambda,i}|, \quad \text{for } i = 1, 2, \ldots, \Omega. \tag{A.35}$$

$$\iff \quad |\lambda^n| < 1 \quad \iff \quad |\lambda| < 1. \tag{A.36}$$

Case2: $\sum_{i=1}^{\Omega} |u_{\lambda,i}| = |\sum_{i=1}^{\Omega} u_{\lambda,i}|$**.**

We have

$$\sum_{i=1}^{\Omega} \sum_{j=1}^{\Omega} \left(\hat{T}^n\right)_{ij} u_{\lambda,j} = \sum_{j=1}^{\Omega} u_{\lambda,j} = \lambda^n \sum_{i=1} u_{\lambda,i}. \tag{A.37}$$

$$\iff \quad \lambda^n = 1 \quad (\because \boldsymbol{u}_\lambda \neq \boldsymbol{0}, u_{\lambda,i} \geq 0 \Rightarrow \sum_{i=1}^{\Omega} u_{\lambda,i} > 0). \tag{A.38}$$

Thus there is only an eigenvalue 1 with its absolute value 1. □

Theorem A.2.5. The vector $\lim_{N\to\infty} \hat{T}^N \boldsymbol{r} = \boldsymbol{0}$ for any $\boldsymbol{r} \in \mathbb{C}$ is orthogonal to $\boldsymbol{d}$.

Proof. For an arbitrary vector $\boldsymbol{r}$, we can decompose it into its real and imaginary parts as

$\boldsymbol{r} = \boldsymbol{r}_{\mathrm{R}} + i\boldsymbol{r}_{\mathrm{I}}$. Since the condition $(\boldsymbol{r}, \boldsymbol{d}) = 0$ is equivalent to $\sum_{i=1}^{\Omega} r_i = 0$, we have

$$\sum_{j \in I_+} r_j + \sum_{j \in I_-} r_j = 0, \tag{A.39}$$

where $I_\pm := \{j \mid r_j \gtrless 0, 1 \leq j \leq \Omega\}$. Note that $\sum_{j \in I_+} r_j = \sum_{j \in I_-} |r_j|$. Thus we have

$$\sum_{j \in I_+} r_j = \sum_{j \in I_-} |r_j| = \|\boldsymbol{r}\|_1 / 2. \tag{A.40}$$

Since $\hat{T}$ is strongly connected, there is an integer N_0 such that $\left(\hat{T}^{N_0}\right)_{ij} > 0$ for an arbitrary $1 \leq i, j \leq \Omega$. For the N_0 we have

$$\left(\hat{T}^{N_0}\boldsymbol{r}\right) = \sum_{j=1}^{\Omega} \left(\hat{T}^{N_0}\right)_{ij} r_j = \sum_{j \in I_+} \left(\hat{T}^{N_0}\right)_{ij} r_j - \sum_{j \in I_-} \left(\hat{T}^{N_0}\right)_{ij} |r_j| \tag{A.41}$$

$$= \sum_{j=1}^{\Omega} \left(\hat{T}^{N_0}\right)_{ij} r_j - 2 \sum_{j \in I_-} \left(\hat{T}^{N_0}\right)_{ij} |r_j| \tag{A.42}$$

$$\leq \sum_{j=1}^{\Omega} \left(\hat{T}^{N_0}\right)_{ij} r_j - 2\delta_{N_0} \sum_{j \in I_-} |r_j| \tag{A.43}$$

$$= \sum_{j=1}^{\Omega} \left(\hat{T}^{N_0}\right)_{ij} r_j - \delta_{N_0} \|\boldsymbol{r}\|_1, \tag{A.44}$$

where $\delta_{N_0} := \min_{1 \leq i,j \leq \Omega} \left[\left(\hat{T}^{N_0}\right)_{ij}\right]$ (for $i = 1, 2, \ldots, \Omega$). Note that there exists a $\delta_{N_0} > 0$ for the

strongly connected matrix $\hat{T}$. Similarly we have

$$\left(\hat{T}^{N_0}\boldsymbol{r}\right) = \sum_{j=1}^{\Omega}\left(\hat{T}^{N_0}\right)_{ij} r_j = \sum_{j\in I_+}\left(\hat{T}^{N_0}\right)_{ij} r_j - \sum_{j\in I_-}\left(\hat{T}^{N_0}\right)_{ij} |r_j| \tag{A.45}$$

$$=2\sum_{j\in I_+}\left(\hat{T}^{N_0}\right)_{ij} r_j - \sum_{j=1}^{\Omega}\left(\hat{T}^{N_0}\right)_{ij} |r_j| \tag{A.46}$$

$$\geq 2\delta_{N_0}\sum_{j\in I_+} r_j - \sum_{j=1}^{\Omega}\left(\hat{T}^{N_0}\right)_{ij} |r_j| \tag{A.47}$$

$$=\delta_{N_0}\|\boldsymbol{r}\|_1 - \sum_{j=1}^{\Omega}\left(\hat{T}^{N_0}\right)_{ij} |r_j|, \quad (\text{for } i = 1, 2, \ldots, \Omega). \tag{A.48}$$

Combining them, we have

$$|\left(\hat{T}^{N_0}\boldsymbol{r}\right)| \leq \sum_{j=1}^{\Omega}\left(\hat{T}^{N_0}\right)_{ij} |r_j| - \delta_{N_0}\|\boldsymbol{r}\|_1, \quad (\text{for } i = 1, 2, \ldots, \Omega), \tag{A.49}$$

and then it holds that

$$\|\hat{T}^{N_0}\boldsymbol{r}\|_1 = \sum_{i=1}^{\Omega}|\left(\hat{T}^{N_0}\boldsymbol{r}\right)_i| \leq \sum_{j=1}^{\Omega}|r_j| - N_0\delta_{N_0}\|\boldsymbol{r}\|_1 = (1 - N\delta_{N_0})\|\boldsymbol{r}\|_1. \tag{A.50}$$

The vector $\hat{T}^{N_0}\boldsymbol{r}$ is also orthogonal to the vector $\boldsymbol{d}$, actually it holds that

$$\left(\hat{T}^{N_0}\boldsymbol{r}, \boldsymbol{d}\right) = \left(\boldsymbol{r}, {}^{\mathrm{t}}\left(\hat{T}^{N_0}\right)\boldsymbol{d}\right) = \left(\boldsymbol{r}, \left({}^{\mathrm{t}}\hat{T}\right)^{N_0}\boldsymbol{d}\right) = (\boldsymbol{r}, \boldsymbol{d}) = 0. \tag{A.51}$$

Then, for any positive integer l, we can repeat this discussion as

$$\|\hat{T}^{N_0 l}\boldsymbol{r}\|_1 \leq (1 - N_0\delta_{N_0})^l\|\boldsymbol{r}\|_1. \tag{A.52}$$

Since $N_0 > 0, \delta_{N_0} > 0$ and thus $1 - N_0\delta_{N_0} < 0$, we have

$$\lim_{l\to\infty}(1 - N_0\delta_{N_0})^l\|\boldsymbol{r}\|_1 = 0. \tag{A.53}$$

$$\iff \quad \lim_{l\to\infty}\|\hat{T}^{N_0 l}\boldsymbol{r}\|_1 = 0. \tag{A.54}$$

Thus, for an arbitrary positive integer N, we have

$$\lim_{N\to\infty}\|\hat{T}^N\boldsymbol{r}\|_1 = 0. \tag{A.55}$$

□

Theorem A.2.6. We can write any vector $\boldsymbol{x}$ as the superposition of $\boldsymbol{u}_1$ and $\boldsymbol{r}$.

Proof. Defining the coefficient $c_{1,\boldsymbol{x}} := (\boldsymbol{x}, \boldsymbol{d})/(\boldsymbol{u}_1, \boldsymbol{d})$ and the vector $\boldsymbol{r}_{\boldsymbol{x}} := \boldsymbol{x} - c_{1,\boldsymbol{x}}\boldsymbol{u}_1$, we have

$$(\boldsymbol{r}_{\boldsymbol{x}}, \boldsymbol{d}) = (\boldsymbol{x}, \boldsymbol{d}) - \frac{(\boldsymbol{x}, \boldsymbol{d})}{(\boldsymbol{u}_1, \boldsymbol{d})}(\boldsymbol{u}_1, \boldsymbol{d}) = 0, \tag{A.56}$$

$$\boldsymbol{x} = c_{1,\boldsymbol{x}}(\boldsymbol{u}_1, \boldsymbol{d}) + \boldsymbol{r}_{\boldsymbol{x}}. \tag{A.57}$$

□

Theorem A.2.7. The limit $\lim_{N\to\infty}\hat{T}^N\boldsymbol{p}^{(0)}$ is independent on the initial vector $\boldsymbol{p}^{(0)}$ and it holds that

$$\lim_{N\to\infty}\hat{T}^N\boldsymbol{p}^{(0)} = \frac{\boldsymbol{u}_1}{\|\boldsymbol{u}_1\|_1}, \tag{A.58}$$

where the vector $\boldsymbol{p}^{(0)} = {}^{\mathrm{t}}\left\{p_1^{(0)}, p_2^{(0)}, \ldots, p_\Omega^{(0)}\right\}$ is in the class of probability vectors and then it is normalized $\sum_{i=1}^{\Omega} p_i^{(0)} = 1$.

Proof. From the theorem A.2.6, we have

$$\hat{T}^N \boldsymbol{p}^{(0)} = c_{1,\boldsymbol{p}^{(0)}} \hat{T}^N \boldsymbol{u}_1 + \hat{T}^N \boldsymbol{r}_{\boldsymbol{p}^{(0)}} = c_{1,\boldsymbol{p}^{(0)}} \boldsymbol{u}_1 + \hat{T}^N \boldsymbol{r}_{\boldsymbol{p}^{(0)}}. \tag{A.59}$$

Its limit $N \to \infty$ is taken as

$$\lim_{N\to\infty} \hat{T}^N \boldsymbol{p}^{(0)} = c_{1,\boldsymbol{p}^{(0)}} \boldsymbol{u}_1 + \lim_{N\to\infty} \hat{T}^N \boldsymbol{r}_{\boldsymbol{p}^{(0)}} = c_{1,\boldsymbol{p}^{(0)}} \boldsymbol{u}_1. \tag{A.60}$$

Using the matrix $\hat{A} := {\boldsymbol{u}_1}^{\mathrm{t}} \boldsymbol{d}/(\boldsymbol{u}_1, \boldsymbol{d})$, we have

$$\left(\hat{A}\boldsymbol{p}^{(0)}\right)_i = \sum_{j=1}^{\Omega} \frac{(\boldsymbol{u}_1)_i}{(\boldsymbol{u}_1, \boldsymbol{d})} \left(\boldsymbol{p}^{(0)}\right)_j = \left(\boldsymbol{p}^{(0)}, \boldsymbol{d}\right) \frac{(\boldsymbol{u}_1)_i}{(\boldsymbol{u}_1, \boldsymbol{d})}, \quad \text{for } i = 1, 2, \ldots, \Omega. \tag{A.61}$$

Then it leads

$$\hat{A}\boldsymbol{p}^{(0)} = \frac{(\boldsymbol{u}_1)_i}{(\boldsymbol{u}_1, \boldsymbol{d})} \boldsymbol{p}^{(0)} = c_{1,\boldsymbol{p}^{(0)}} \boldsymbol{p}^{(0)}. \tag{A.62}$$

Then the limit $N \to \infty$ for $\hat{T}^N \boldsymbol{p}^{(0)}$ is rewritten by a simple multiplication as follows

$$\lim_{N\to\infty} \hat{T}^N \boldsymbol{p}^{(0)} = \frac{{\boldsymbol{u}_1}^{\mathrm{t}} \boldsymbol{d}}{(\boldsymbol{u}_1, \boldsymbol{d})} \boldsymbol{p}^{(0)}. \tag{A.63}$$

The expression (A.63) lead to the relation $\lim_{N\to\infty} \hat{T}^N \boldsymbol{p}^{(0)} = \boldsymbol{u}_1/\|\boldsymbol{u}_1\|_1$. Actually it holds that

$$\frac{{\boldsymbol{u}_1}^{\mathrm{t}} \boldsymbol{d}}{(\boldsymbol{u}_1, \boldsymbol{d})} \left(\boldsymbol{p}^{(0)}\right)_i = \frac{\sum_{j=1}^{\Omega} (\boldsymbol{u}_1)_i (\boldsymbol{d})_j \left(\boldsymbol{p}^{(0)}\right)_j}{(\boldsymbol{u}_1, \boldsymbol{d})} = \frac{u_{1,i}}{\|\boldsymbol{u}_1\|_1}, \tag{A.64}$$

thus we have

$$\lim_{N\to\infty} \hat{T}^N \boldsymbol{p}^{(0)} = \frac{\boldsymbol{u}_1}{\|\boldsymbol{u}_1\|_1}. \tag{A.65}$$

□

Once we get a strongly connected stochastic matrix $\hat{T}$, its stationary distribution $\boldsymbol{u}_1/\|\boldsymbol{u}_1\|_1$ is determined independently on the initial distribution. We can consider this procedure as a *transformation* from the matrix $\hat{T}$ into the vector $\boldsymbol{u}_1/\|\boldsymbol{u}_1\|_1$.

A.3 Construction of the Stochastic Matrix based on the Detailed Balanced Condition

On the other hand, we can also consider the inverse transformation. This means the *construction* of the matrix $\hat{T}'$ with a *desired* stationary distribution $\boldsymbol{p}'$. We can actually formulate such the procedure using the *detailed balanced condition* as follows.

Definition A.3.1. If a vector $\boldsymbol{p}' = {}^{\mathrm{t}}(p'_1, p'_2, \ldots, p'_\Omega)$ is the stationary distribution of the stochastic matrix $\hat{T}' = \left(T'_{ij}\right)$, it holds that

$$T'_{ij}p'_j = T'_{ji}p'_i \tag{A.66}$$

for $1 \leq i, j \leq \Omega$.

This property is simplified by summing over the subscription i as follows

$$\sum_{i=1}^{\Omega} T'_{ij}p'_j = p'_j = \sum_{i=1}^{\Omega} T'_{ji}p'_i = \left(\hat{T}\boldsymbol{p}'\right)_j, \quad \text{for } j = 1, 2, \ldots, \Omega. \tag{A.67}$$

Then if the detailed balanced condition holds for a matrix $\hat{T}'$, the corresponding vector $\boldsymbol{p}'$ is the fixed point of the matrix $\hat{T}'$. Thus in order to get the matrix $\hat{T}'$ which lead any distribution $\boldsymbol{p}^{(0)}$ to the desired distribution $\boldsymbol{p}'$, we only have to construct each element T'_{ij} of the matrix according to the condition (A.66) and make the matrix strongly connected.

In Monte Carlo simulations of statistical mechanics, we calculate the equilibrium distribution $\boldsymbol{p}_{\rm eq}(\beta)$ at an inverse temperature β using an initial state i_0 and a rule of the stochastic process $i \to j \to j' \to \ldots$. We can regard the matrix construction method as a set of the stochastic process $i_0 \to j \to j' \to \ldots$ over all possible states $i_0 = 1, 2, \ldots, \Omega$. In other words, the matrix T_{ij} corresponding to a simulation contains the information of all possible initial states $i_0 = 1, 2, \ldots, \Omega$ and all possible transitions $T_{1,i_0}, T_{2,i_0}, \ldots, T_{\Omega,i_0}$ respectively from them. Thus we often consider a *sample path* by an appropriate initial state and the matrix.

The condition (A.66) or

$$\frac{T_{ij}}{T_{ji}} = \frac{p_i}{p_j} \tag{A.68}$$

is not sufficient to determine a concrete form of the matrix $\hat{T}$ and thus in general there is a degree of freedom in the form of $\hat{T}$. For Monte Carlo simulations of equilibrium statistical mechanics, this freedom also remains as follows:

$$\frac{T_{ij}(\beta)}{T_{ji}(\beta)} = \frac{p_i(\beta)}{p_j(\beta)} = \mathrm{e}^{-\beta(E_i - E_j)}, \quad \text{for } 1 \le i, j \le \Omega, \tag{A.69}$$

where $T_{ij}(\beta)$ and $p_i(\beta)$ are the matrix corresponding to a simulation and the probability that the i-th state emerges respectively with a fixed inverse temperature β. But this relation is important that the rate of transition probabilities is always given by a difference of energy eigenvalues $\{E_1, E_2, \ldots, E_\Omega\}$, and thus we do *not* have to calculate exact values of $\tilde{p}_i(\beta) :=$

$\exp[-\beta E_i]/Z(\beta)$ ($Z(\beta) := \sum_i \exp[-\beta E_i]$).

If we use the Metropolis probability for the N-spins system, each element of the matrix $(T_{ij}(\beta))$ is written as follows.

$$T_{ij}(\beta) = \begin{cases} \frac{1}{N}\min\left[1, \mathrm{e}^{-\beta(E_i - E_j)}\right] & \text{for states } i,j \text{ mutually reacheable by a single flip,} \\ 0 & \text{for states } i,j \textit{ not} \text{ mutually reacheable by a single flip.} \end{cases} \tag{A.70}$$

The factor $1/N$ describes the equivalent selection of a spin to flip.

We call the matrix with the condition (A.70) *Metropolis matrix* and denote by $(M_{ij}) := (T_{ij}(\beta))\,|_{(\mathrm{A.70})}$ from now on.

Metropolis matrices generally have few non-zero elements due to not taking transitions between all energy eigenstates into account. Thus the Monte Carlo simulation with Metropolis rate is very simple in terms of its algorithm, but the convergence is not trivial. In following subsections, we show that the convergence for quite limited cases using a strong connectivity of the stochastic matrix.

A.3.1 Metropolis Matrix for the Model of the Size 2×2

We constructed the Metropolis matrix $\hat{M}^{[2,2]}(\beta)$ for the model of size $L_x = 2, L_z = 2$ in a concrete form and verified that all elements of the fourth power of the matrix are non-zero.

By the fact, we can see the existence of its unique stationary state as the long-time limit . In addition we investigated the distribution of the eigenvalues of $\hat{M}^{[2,2]}(\beta)$ for several temperatures and verified that the matrix $\hat{M}^{[2,2]}(\beta)$ has only an eigenvalue 1 and eigenvalue all inner than unit circle on the complex plane except for the case $\beta = 0$ (See Figure A.2).

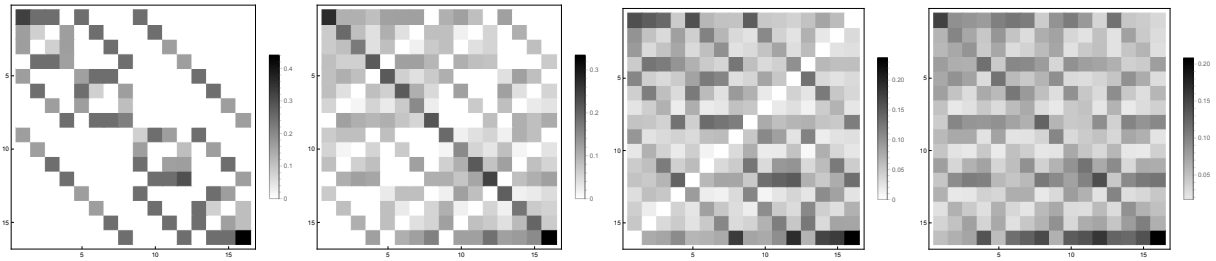

(a) $\hat{M}_{[2,2]}(\beta)$ (b) $\left\{\hat{M}_{[2,2]}(\beta)\right\}^2$ (c) $\left\{\hat{M}_{[2,2]}(\beta)\right\}^3$ (d) $\left\{\hat{M}_{[2,2]}(\beta)\right\}^4$

Figure A.1: The array plots of powers of $\hat{M}_{[2,2]}(\beta)$.

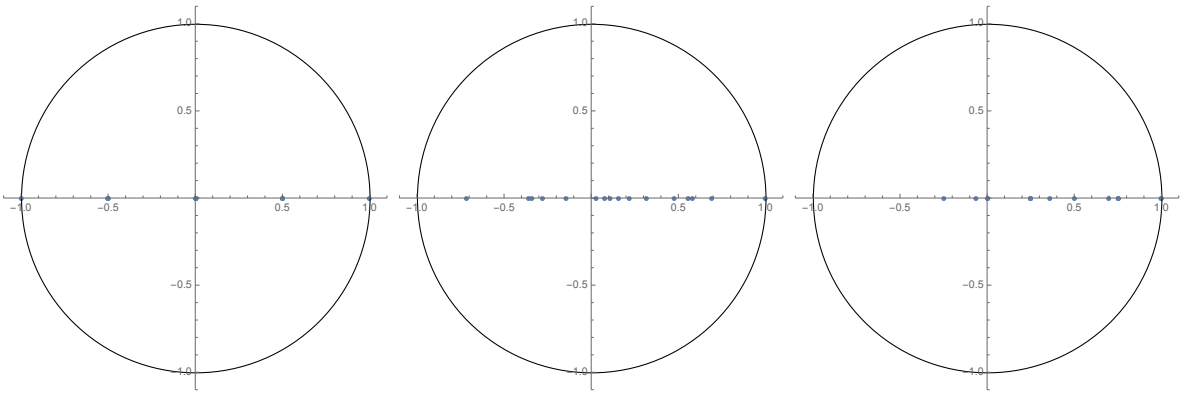

(a) $\beta = 0$ (b) $\beta = 0.1$ (c) $\beta = \infty$

Figure A.2: The distributions of eigenvalues for $\hat{M}^{[2,2]}(\beta)$.

A.4 Stochastic Matrices and Non-Equilbrium Monte Carlo Simulations

We extended the Metropolis matrix which we constructed in the previous subsection to construct a new type of stochastic matrix, which corresponds to the model of magnetic friction.

$$\hat{T}^{[L_x,L_z]}(\beta,v) := \left[\left\{\hat{M}^{[L_x,L_z]}(\beta)\right\}^{\frac{L_x\times L_z}{v}} \hat{S}^{[L_x,L_z]}\right]^v \quad v \in \{\text{Divisors of } Lx\times Lz\}, \tag{A.71}$$

where the matrix $\hat{S}^{[L_x,L_z]}$ expresses the operation of sliding the model of size $L_x \times L_z$ by a lattice constant, and possesses the similar structure of elements to the unit matrix (See Figure A.3).

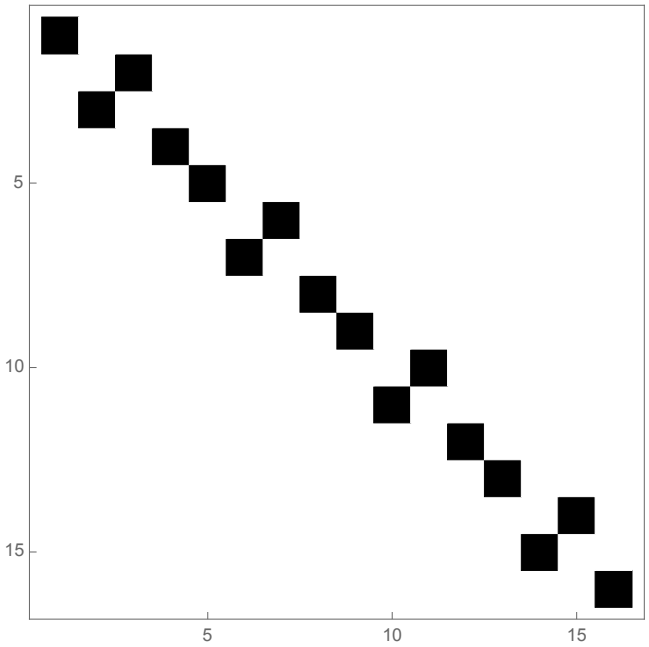

Figure A.3: The array plot of $\hat{S}^{[2,2]}$.

The matrix $\hat{T}^{[L_x,L_z]}(\beta,v)$ describes a time evolution for a MC sweeps, because the matrix have the $L_x \times L_z$-th power of $\hat{M}^{[L_x,L_z]}(\beta)$. The task of diagonalizing the Matrix $\hat{T}^{[L_x,L_z]}(\beta,v)$ is same as that of $\left\{\hat{M}^{[L_x,L_z]}(\beta)\right\}^{\frac{L_x\times L_z}{v}} \hat{S}^{[L_x,L_z]}$[1]. The matrix $\left\{\hat{M}^{[L_x,L_z]}(\beta)\right\}^{\frac{L_x\times L_z}{v}} \hat{S}^{[L_x,L_z]}$ is also

[1]This corresponds to a time evolution for $1/v$ MC sweeps.

strongly connected and thus have a unique stationary state (See Figure FigNum). The distribution of eigenvalues of $\left\{\hat{M}^{[L_x,L_z]}(\beta)\right\}^{\frac{L_x\times L_z}{v}}\hat{S}^{[L_x,L_z]}$ is similar to that of $\left\{\hat{M}^{[L_x,L_z]}(\beta)\right\}^{\frac{L_x\times L_z}{v}}$.

Appendix B

Results of Simulations in More Detail

B.1 Checking the Convergence in the Limit $L_x \to \infty$

We now demonstrate that following two observables are converging at corresponding numerical large size limits.

$$f(L_z, T) := \lim_{L_x \to \infty} \frac{F(L_x, L_z, T)}{L_x} \tag{B.1}$$

$$\epsilon_{\mathrm{b}}(L_z, T) := \lim_{L_x \to \infty} \frac{E_b(L_x, L_z, T)}{L_x L_z} \tag{B.2}$$

Both of them have no dependence on L_x and also do not diverge in the limit of L_z. Thus we can analyze these qualitative and pure dependence on L_z and T. We use the aspect of $L_x = 10L_z, 20L_z, \ldots, 50L_z$ for checking the convergence in the limit $L_x/L_z \to \infty$ with fixed L_z.

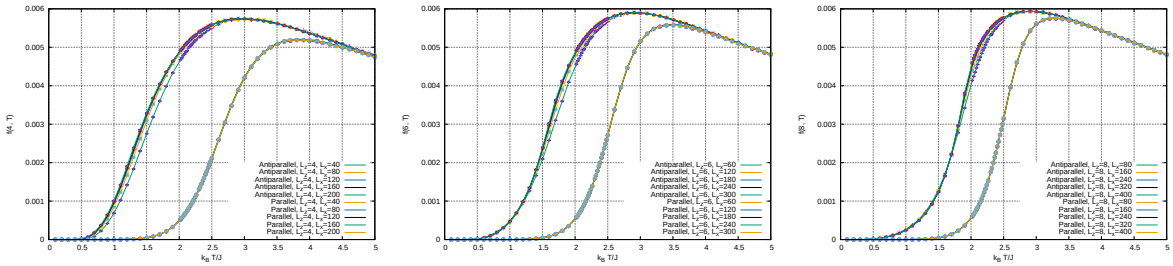

(a) $L_z = 4$ (b) $L_z = 6$ (c) $L_z = 8$

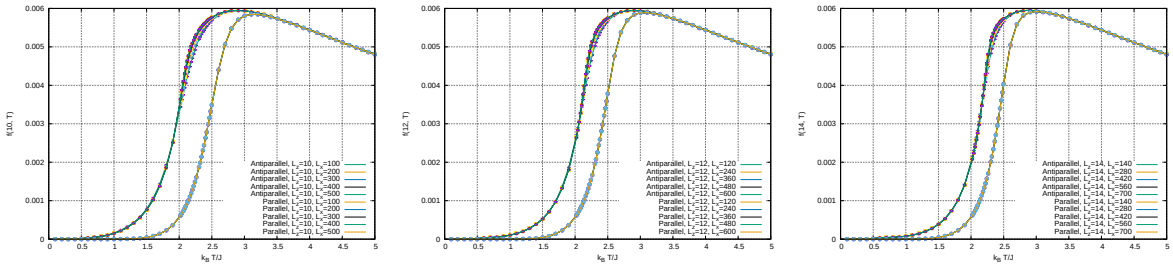

(d) $L_z = 10$ (e) $L_z = 12$ (f) $L_z = 14$

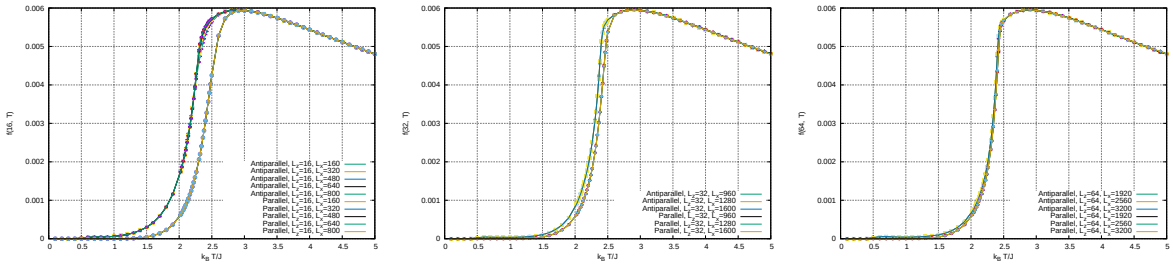

(g) $L_z = 16$ (h) $L_z = 32$ (i) $L_z = 64$

Figure B.1: Each data shows $F(L_x, L_z, T)/L_x$ versus T.

B.1.1 Dependence of $F(L_x, L_z, T)/L_x$ on L_x for each L_z

We show that the quantity $F(L_x, L_z, T)/L_x$ has no dependence on L_x at a sufficient large L_x for each L_z. The following graphs are the temperature dependence of the frictional force density with each of boundary conditions along the z-direction for each of longitudinal size $L_z = 4, 6, 8, 10, 12, 14, 16$ (fig.B.1).

B.1.2 Dependence of $E_{\rm b}(L_x, L_z, T)/(L_x L_z)$ on L_x for each L_z

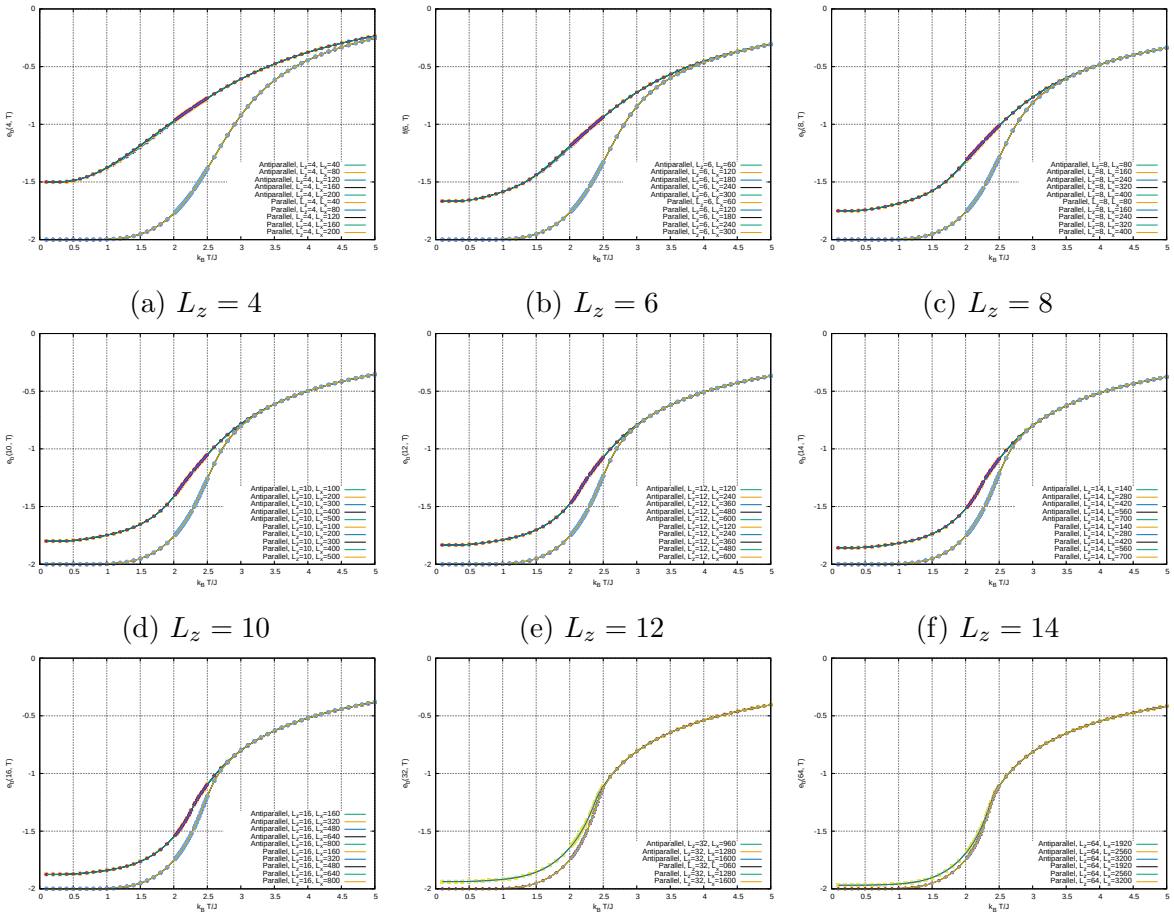

(a) $L_z = 4$ (b) $L_z = 6$ (c) $L_z = 8$

(d) $L_z = 10$ (e) $L_z = 12$ (f) $L_z = 14$

(g) $L_z = 16$ (h) $L_z = 32$ (i) $L_z = 64$

Figure B.2: Each data shows $E(L_x, L_z, T)/(L_x L_z)$ versus T.

We show that the quantity $E_{\rm b}(L_x, L_z, T)/L_x$ has no dependence on L_x at a sufficient large L_x for each L_z. The following graphs are the temperature dependence of the frictional force density with each of boundary conditions along the z-direction for each of longitudinal size

$L_z = 4, 6, 8, 10, 12, 14, 16$ (fig.B.2).

Bibliography

[1] Dirk Kadau, Alfred Hucht, and Dietrich E. Wolf. Magnetic Friction in Ising Spin Systems. *Phys. Rev. Lett.*, 101(13):137205, sep 2008.

[2] Alfred Hucht. Non-equilibrium phase transition in an exactly solvable driven Ising model with friction. *Phys. Rev. E*, 80(6):061138, sep 2009.

[3] M. P. Magiera, L. Brendel, D. E. Wolf, and U. Nowak. Spin excitations in a monolayer scanned by a magnetic tip. *EPL (Europhysics Lett.*, 87(2):26002, 2009.

[4] Martin P. Magiera, Sebastian Angst, Alfred Hucht, and Dietrich E. Wolf. Magnetic friction: From Stokes to Coulomb behavior. *Phys. Rev. B*, 84(21):212301, dec 2011.

[5] Martin P. Magiera, L. Brendel, D. E. Wolf, and U. Nowak. Spin waves cause non-linear friction. *Europhys. Lett.*, 95:17010, 2011.

[6] Roy J. Glauber. Time-Dependent Statistics of the Ising Model. *J. Math. Phys.*, 4(2):294, 1963.